ENSO and the carbon cycle

Richard Betts, Chantelle Burton, Richard Feely, Mat Collins, Chris Jones, Andy Wiltshire

Chapter in AGU Monograph "ENSO in a changing climate" – McPhadden, Cai and Santoso

Abstract

1. Observational studies of atmospheric CO2, land ecosystem and ocean processes show that variability in the carbon cycle is closely related with ENSO. Years with a warm anomaly in the tropical Pacific show a faster CO2 rise due to weaker land carbon sinks, particularly in the tropics, with a partial offset by stronger net uptake by oceans. The opposite happens in years with cool Pacific SST anomalies. This relationship holds for small ENSO SST anomalies as well as large ones, and is robust enough for the annual CO2 growth rate anomaly to be highly predictable on the basis of SST observations and forecasts. Generally, variability in the land-atmosphere carbon flux is mainly driven by physiological processes â€“ photosynthesis and/or respiration â€“ with a smaller contribution from fire. Fire was important in the 1997-98 El NiÃ±o, making a major contribution to the CO2 rise which can be viewed as anthropogenic in nature since the ignition was caused by humans. However, in the 2015-16 El NiÃ±o event, the change in land carbon flux was mainly due to physiological processes, particularly reduced productivity. In the oceans, El NiÃ±o conditions involve decreased upwelling of carbon in the equatorial Pacific due to a weakening of the trade winds, causing this region to become a weaker sink of CO2 or near-neutral if the El NiÃ±o event is strong. The year-to-year variations in the rate of CO2 rise can be successfully reconstructed and predicted on the basis of sea surface temperatures in the Pacific. ENSO-CO2 relationships may also provide an emergent constraint on the strength of climate-carbon cycle feedbacks on future anthropogenic climate change.

2. Introduction

Climate variability related to ENSO plays an important part in the global carbon and influences the rate at which anthropogenic emissions of CO_2 build up in the atmosphere year to year.

The long-term increase in atmospheric CO_2 concentrations is entirely the result of human-caused emissions of carbon dioxide into the atmosphere – more than enough CO_2 is being emitted by fossil fuel burning, cement production and deforestation to account for the increase measured in the atmosphere (Figure 1). CO_2 concentrations have increased from 278 parts per million (ppm) (Keeling *et al.*, 2001) and passed 410ppm in 2019. This increase would have been even larger if some CO_2 had not been removed from the atmosphere by global vegetation and the oceans. On average these natural sinks together offset approximately half of anthropogenic emissions (Figure 1), although their magnitude varies substantially from year to year (Rayner and Law, 1999). In 2015, for example, natural land and ocean sinks offset less than 40% of anthropogenic emissions (Figure 1).

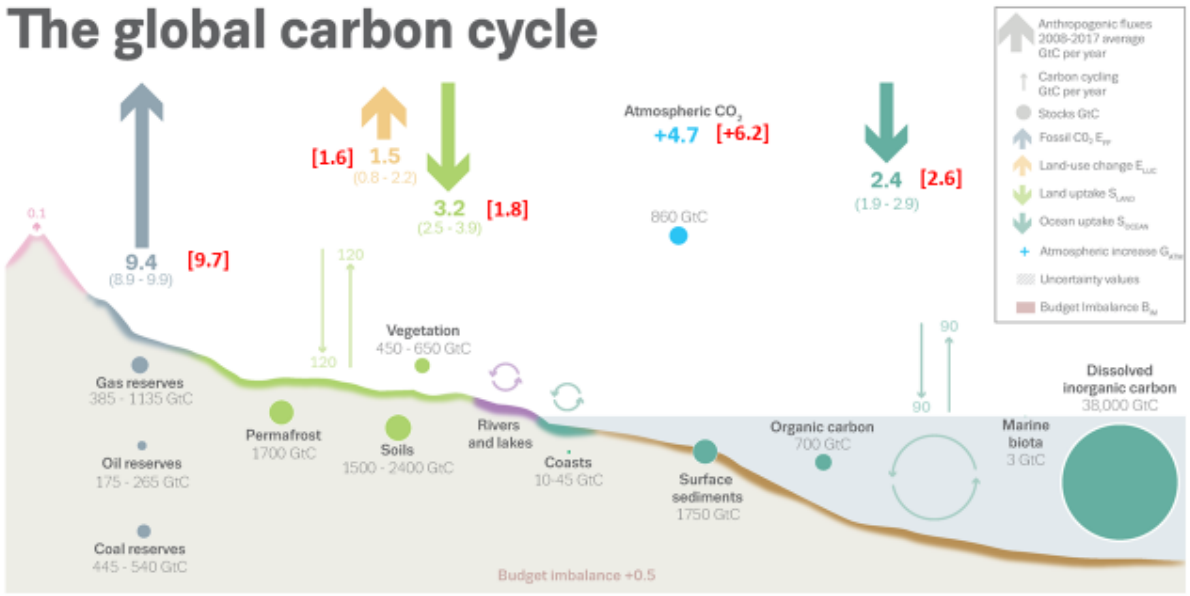

Figure 1. Components of the global carbon cycle on average and in a year with a strong El Niño event. Coloured numbers at heads of arrows are means over 2008-2017. Red numbers in square brackets are values for 2015. Modified from original figure by Le Quéré *et al*., (2018).

It has long been established that the strong interannual variability in the global carbon cycle is related to ENSO (Bacastow, 1976; Bacastow *et al.*, 1985; Keeling and Revelle, 1985; Jones *et al*., 2001). There are clear correlations between the growth rate of atmospheric CO_2 and sea surface temperatures in the regions of the Pacific used as metrics for ENSO, and there is a long history of study of this relationship and the reasons behind it. The tropical regions, particularly land ecosystems have been identified as a key part of the process (Rayner *et al*., 1999)

More recently, measurements of other components of the carbon cycle from an increasing range and variety of sources have provided further evidence for relationships between the carbon cycle and ENSO, and helped improved understanding of the processes involved. Much of this has been on tropical land ecosystems, although the ocean and other land regions are also covered in some datasets.

The large El Niño of 2015/2016 provided a particularly important opportunity to study carbon cycle responses to ENSO, and this has resulted in a wealth of new papers, including a number which arose from a discussion meeting at the Royal Society, London, in November 2017 (Malhi *et al.*, 2018). Many of these provide important input to this chapter. Furthermore, comparisons with the 1997/98 El Niño show differences in the processes involved in the carbon cycle response to these events. For example, in 1997/98, widespread dry and warm conditions across the tropics caused reduced gross primary productivity (GPP) and increased ecosystem respiration, whereas in 2015/16, wetter conditions in parts of Africa caused

increased GPP which partly offset decreases elsewhere (Wang *et al*., 2018). Also, fire emissions from South East Asia played a major role in 1997/98, whereas they were much less substantial in 2015/16.

In addition to contributing to our understanding of the processes of the global carbon cycle and its interactions with the atmosphere and oceans (and their coupled behaviour), insights into ENSO-carbon cycle interactions may also be important for our ability to predict future climate change. For example, if the frequency and/or magnitude of ENSO changes as a result of anthropogenic climate change, this could act as a feedback on CO_2 rise and climate change. More generally, even if ENSO itself does not change, similar processes, teleconnections and regional climate changes may nevertheless be associated with a long-term climate change trend, and hence insights into their impacts on the carbon cycle will be important.

Early work with Earth System Models (ESMs) on climate-carbon cycle feedbacks (Cox *et al*., 2000) discussed the concept of "El Niño-like climate change" (Meehl and Washington*.,* 1996) and the reproduction of observed relationships SSTs in the equatorial pacific and regional climate responses relevant to carbon cycle impacts (such as precipitation in the Amazon region) was used as supporting evidence for the credibility of models projecting strong carbon cycle feedbacks (Cox *et al*., 2004). Moreover, changes in the ENSO regime are also proposed as a potential Tipping Point in the climate system, with possible implications for tropical land ecosystems and the carbon cycle (Kriegler *et al*., 2009). The performance of ESMs in simulating ENSO-carbon cycle interactions on interannual timescales may therefore provide insight into the role of ENSO-related processes in carbon cycle feedbacks on anthropogenic climate change in the longer term.

In this chapter, we give an overview of variability in the global carbon cycle in relation to ENSO. We begin by describing and quantifying the observed interannual and decadal variability in the global carbon cycle, including atmosphere, land and ocean components, and how these correlates with variability in metrics for ENSO. We then discuss the processes through which ENSO impacts on the carbon cycle on interannual timescales. We present an estimate of the impacts of two major ENSO events, 1997/98 and 2015/16, on the annual rise in atmospheric CO_2, and discuss how knowledge of the relationship between the CO_2 rise and ENSO is now being used to make accurate forecasts of the annual CO_2 rise. Finally we discuss the use of ENSO-carbon cycle interactions on interannual timescales as a constraint on carbon cycle feedbacks on long-term anthropogenic climate change.

3. Carbon cycle variability and its correlation with ENSO

2.1 Atmospheric CO_2 growth rate

Measurements of the atmospheric CO_2 concentration have been taken continuously at Mauna Loa Observatory, Hawaii, since 1958, and are good indicator of global mean CO_2 on annual timescales. When measurements began, the annual mean CO_2 concentration at Mauna Loa was 316 parts per million (ppm). In 2019, annual mean concentrations passed 410 ppm, and continue to rise at an accelerating rate as a result of anthropogenic emissions.

Comparison of the year-by-year increment in atmospheric CO_2 with the rate of anthropogenic emissions reveals two important features: a clear increase in both emissions and

concentrations growth in the long term, but also a large short-term variability in the concentrations growth rate which is not seen in the emissions (Figure 2). There are very few years when the emissions rate has been smaller than the previous year, and such cases have only been a few 10^{th} of a GtC. In contrast, the annual CO_2 increment varies by between 1 and 2 GtC from year to year. It has long been noted that the interannual variability in CO_2 concentration increments relates closely to ENSO, with peaks in the CO_2 increment generally coinciding with warm sea surface temperature (SST) anomalies in the tropical Pacific (Figure 2) (Bacastow, 1976; Bacastow *et al.*, 1985; Keeling and Revelle, 1985). The exception is in years following large volcanic eruptions, particularly Pinatubo in 1991 (Jones *et al*., 2001)

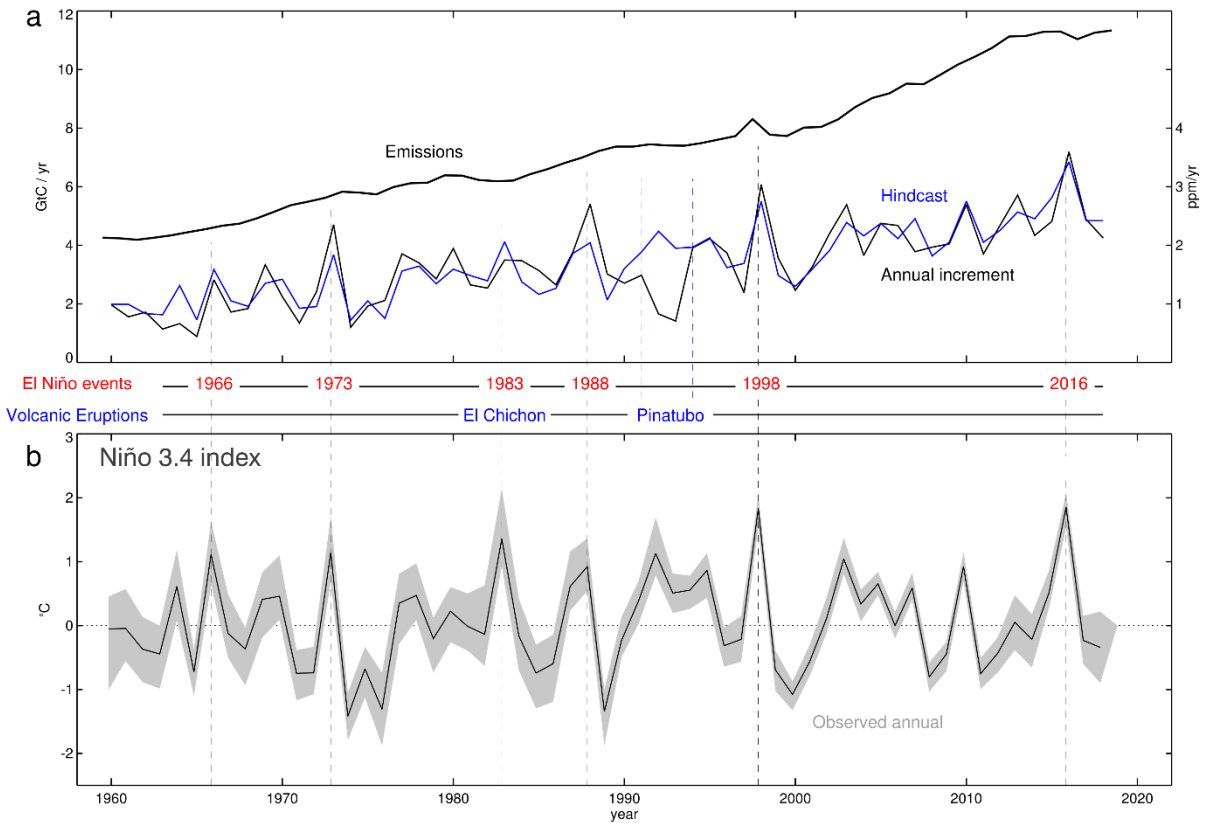

Figure 2. Relationships between annual CO_2 increments at Mauna Loa and sea surface temperatures in the Niño3.4 region of the Pacific, including a statistical reconstruction of the annual increment based on SSTs. (a) Anthropogenic emissions from the Global Carbon Project dataset [Le Quéré, C. et al (2018)] and CO_2 concentrations at Mauna Loa from observations (black) and reconstruction from emissions and SSTs using Equation (1) (blue). (b) Annual mean April-March SSTs from the HadSST3.1.1.0 dataset [Kennedy *et al.*, 2011a, 2011b], with anomalies in °C calculated relative to the 1961-1990 mean.

There is a strong correlation between the annual CO_2 increment and SSTs anomalies in the equatorial Pacific for both large and small variations. The correlation is strongest when annual mean SSTs are taken from April to March (Jones *et al.*, 2001). There are obvious large spikes in CO_2 growth coinciding with El Niño years, and troughs coinciding with La Niña years (Figure 2). The exception to this is when El Niño events coincide with a major volcanic eruption, which temporarily cools the global climate due to the injection of aerosol particles into the atmosphere which reflect some of the incoming solar radiation back to space. It is also clear that generally the CO_2 growth rate relates to Pacific SST anomalies even in years with smaller SST anomalies which are not formally identified as “El Niño” or “La Niña” (Figure 2). Mechanisms of the relationship with the carbon cycle must therefore still be present even when a full ENSO event has not emerged.

As well as the correlation between annual means, apparent relationships between the CO_2 increment and SSTs can also be seen on longer timescales. For example, after the concentration increment increased at approximately half the rate of increase of emissions for the first four decades of the record, from the mid-2000s onwards the annual CO_2 increment ceased to increase for around a decade. The CO_2 increment varied around an average of

approximately 2.1 ppm yr^{-1}, despite emissions rising more rapidly at that time (Keenan *et al*., 2016). This coincided with a period of relatively cool tropical Pacific SSTs, with La Niña episodes in 2007-2009 and 2010-2012 with only small positive SST anomalies in between.

The timeseries of CO_2 increments can be reconstructed from a multiple linear regression of annual CO_2 increments (ΔCO_2) against annual anthropogenic emissions (ε) and the annual mean anomaly in sea surface temperatures in the region of the equatorial Pacific Ocean characterising ENSO activity (*N)* (Jones and Cox, 2005)*:*

$$\Delta CO_2 = \alpha_1 + \alpha_2 N + \alpha_3 \varepsilon \qquad \text{(Equation 1)}$$

Where α_1, α_2 and α_3 are regression coefficients calculated using the observed records of ΔCO_2, N and ε. Table 1 shows values of these coefficients calculated using observed records up to 2017.

Table 1. Regression coefficients for Equation 1 calculated using observed records up to 2017 (Betts *et al*., 2018).

α_1 (ppm yr^{-1})	0.045
α_2 (ppm yr^{-1} °C^{-1})	0.426
α_3 (ppm GtC^{-1})	0.214

This method can successfully reproduce the variability in the observed CO_2 rise (Figure 2) although it has limitations, particularly concerning the choice of the specific region of the Pacific for *N* because the carbon cycle can respond differently to ENSO temperature anomalies occurring in different parts of the equatorial region (Chylek *et al*., 2018). For example, the 1997/98 El Niño was different in character to that of 2015/16, with the temperature anomaly being focussed more in the central Pacific (Niño3 region) in 1997/98 and more in the eastern Pacific (Niño3.4) in 2015/16 (Santoso *et al*., 2017). Jones and Cox (2005) applied Equation 1 using Niño3 SST, whereas Betts *et al.* (2016) used Niño3.4. The hindcast reconstruction in Figure 2 here also uses Niño3.4. Nevertheless, use of either region gives a good reconstruction overall.

2.2 Flows of CO_2 between the atmosphere and surface

The rate of uptake of CO_2 from the atmosphere by the surfaces of the global land and ocean has been increasing over recent decades (Figure 3), with the current rate being approximately 4 GtC yr^{-1}. There is considerable year-to-year variability in this, and while the long-term trend in uptake is similar for both the land and ocean fluxes, the main contribution to interannual variability comes from the land flux. Generally, the atmosphere-land flux temporarily becomes smaller (ie: a weaker net land sink) in El Niño years while the atmosphere-ocean flux temporarily becomes slightly larger (ie: a stronger net ocean sink). Much of the research on quantifying and understanding variability in the carbon cycle in relation to ENSO therefore focusses on the atmosphere-land fluxes, although studying the atmosphere-ocean fluxes is also important.

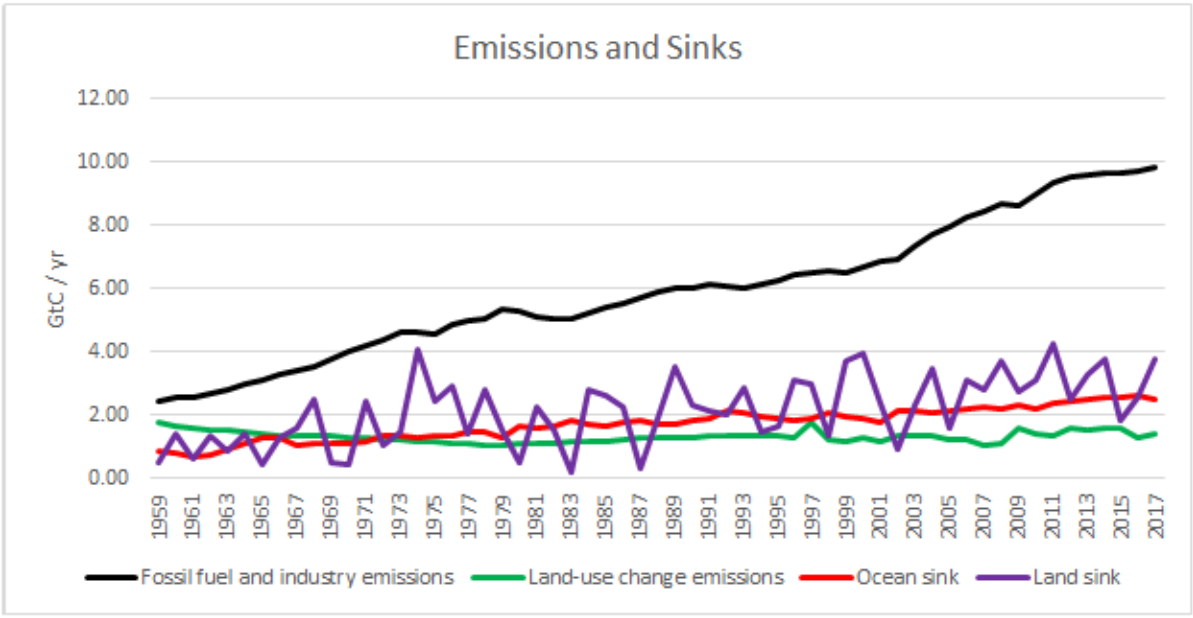

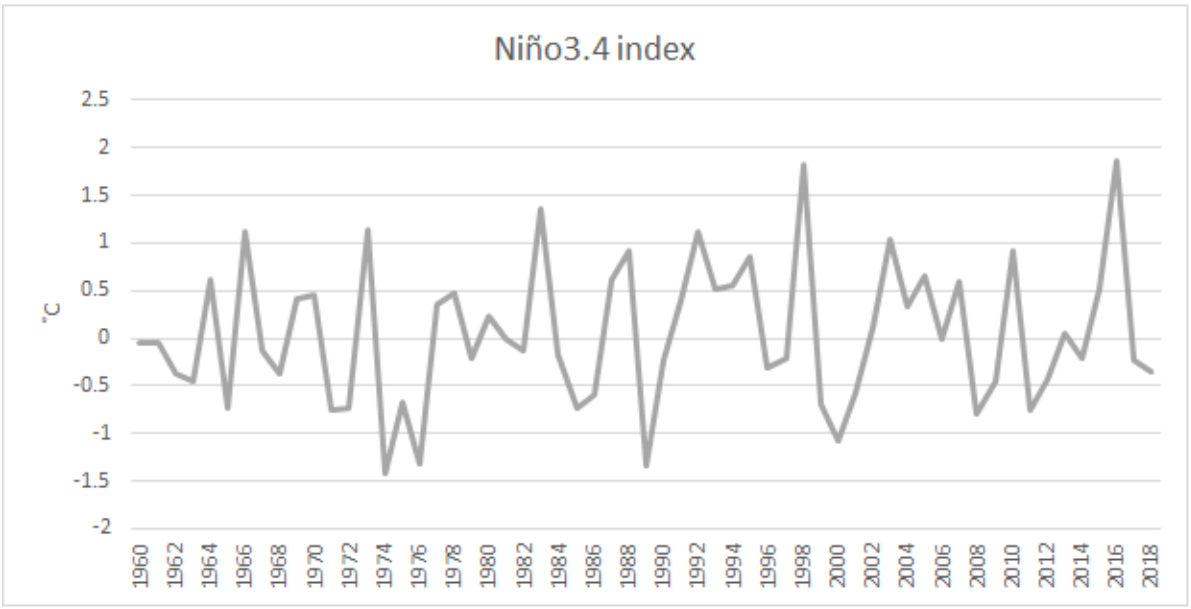

Figure 3. Relationships between components of change in the carbon cycle and sea surface temperatures (SSTs) in the Niño3.4 region of the Pacific. (a) Emissions from fossil fuel burning and land use change separately, and land and ocean carbon sinks (Le Quéré *et al.*, 2018). (c) Annual mean April-March SSTs from the HadSST3.1.1.0 dataset (Kennedy *et al.*, 2011a, 2011b), with anomalies in °C calculated relative to the 1961-1990 mean.

2.2.1 Atmosphere-land CO_2 flows

The flows of CO_2 between the atmosphere and surface can be quantified with inversion modelling, which combines measurements of atmospheric CO_2 concentrations with

atmospheric transport models constrained by observations (eg. Rödenbeck *et al.*, 2018). These simulate the variations in atmosphere-land fluxes both geographically and over time. The net flux of carbon from the atmosphere to land is generally increasing over time, indicating a long-term increase in carbon uptake by land ecosystems. However, the flux becomes stronger in La Niña events and weaker, or even negative, in El Niño events (Figure 3). Broadly similar behaviour is seen both in northern extratropical land and tropical land but with both the trend and interannual variability more marked in the tropics. Overall, land regions take up less CO_2 (or emit more) during El Niño, and take up more CO_2 (or emit less) in La Niña.

In most years since the 1960s, global land ecosystems have been a net sink of carbon, with the mean rate of uptake increasing to over 2 GtC yr^{-1} by the 2010s. However, until 2003, years with El Niño events or smaller warm SST anomalies saw global land ecosystems became a net source of carbon. In 1997-98, the terrestrial biosphere released approximately 2 GtC yr^{-1} to the atmosphere, representing an anomaly of approximately 3 GtC yr^{-1} relative to the long-term mean sink. Most of this was accounted for by emissions from the tropics. After 2003, the long-term increase in global sink strength meant that decreases in the sink strength associated with warm SST anomalies were not enough to turn the terrestrial biosphere into a net source of carbon. Even though the large El Niño of 2015-16 reduced the sink strength substantially, the net land-atmosphere carbon flux remained approximately neutral rather than becoming a net carbon source. The maximum global land sink strength has so far occurred in 2011-2012 and 2013-14, reaching approximately 3 GtC yr^{-1}.

At regional scales, the ENSO response of the atmosphere-land CO_2 flux varies substantially. During El Niño, land south of 25° becomes an overall net source of carbon, and almost all areas of tropical land show positive anomalies (ie: more outgassing of CO_2 (or reduced uptake) from land to the atmosphere; Figure 4). South America includes a particularly strong relative source (or weaker sink), with eastern Amazonia and north-east Brazil showing a major anomaly, especially in the strong El Niño events of 1997 and, to a lesser extent, 2015. Land north of 25° remains an overall carbon sink, but is weaker than average, and some mid- and high-latitude regions show negative anomalies (ie: less CO_2 outgassing, a stronger net carbon sink locally; Figure 4). These general patterns are seen in most El Niño events, but the magnitude of the local anomalies varies between events.

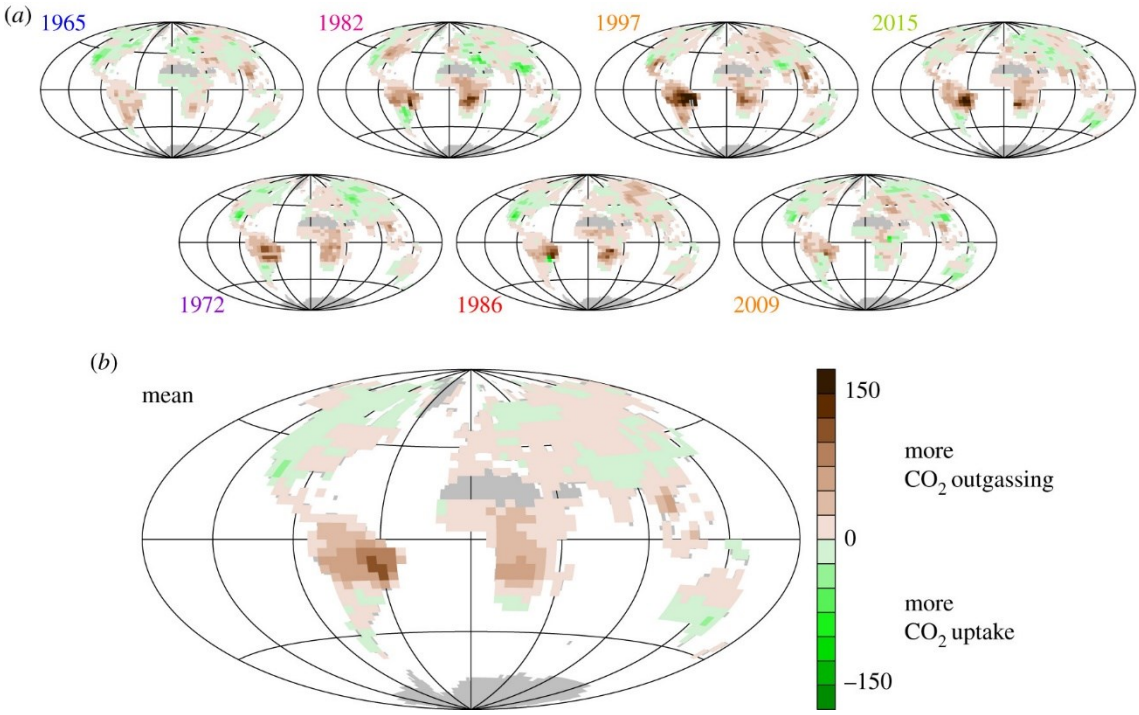

Figure 4. Anomalies in regional land-atmosphere CO_2 fluxes (gC m^{-2} yr^{-1}) during El Niño events, inferred from atmospheric CO_2 observations using a statistical relationship between station CO_2 data and the Multivariate ENSO Index. Reproduced from Rödenbeck *et al*. (2018)

2.2.2 Atmosphere-ocean CO_2 flows

The flux of CO_2 between the atmosphere and ocean is estimated with a number of methods. One method uses the effective partial pressure of CO_2 (the partial pressure pCO_2 corrected to account for CO_2 not behaving as an ideal gas) – measurements are provided by the Surface Ocean CO_2 Atlas (SOCAT; Bakker *et al*., 2016). Another method uses a combined measure of the ratio of oxygen and nitrogen concentrations and CO_2 concentrations, known as Atmospheric Potential Oxygen, is insensitive to changes in CO_2 from the terrestrial biosphere and hence provides a quantification of changes in CO_2 associated with the oceans (Battle *et al*., 2006; Keeling and Manning, 2014). An inversion method combines data-based estimates of anthropogenic CO_2 in the ocean with simulated ocean transport and mixing from ocean general circulation models (Mikaloff Fletcher *et al*., 2006). The distribution of Chlorofluorocarbons (CFCs) in the ocean can also be used to infer CO_2 uptake (McNeil *et al*., 2003). The Global Carbon Project (Le Quéré *et al*. 2018) compiles estimates from all these methods along with estimate from Global Ocean Biogeochemistry Models to produce a combined assessment of atmosphere-ocean CO_2 fluxes (Figure 3c).

The interannual variability in atmosphere-ocean CO_2 fluxes is of the order of a few tenths of a GtC, much less than the variability in atmosphere-land fluxes. Nevertheless, correlations with ENSO are apparent. The global mean atmosphere-ocean CO_2 fluxes respond to ENSO in generally the opposite direction to the atmosphere-land flux response, with an increase in the flux of CO_2 from atmosphere to ocean in El Niño years, and a decrease in La Niña years.

4. Processes involved in ENSO-carbon cycle interactions

3.1 Terrestrial ecosystem processes

The net flow of carbon between the atmosphere and land is known as Net Ecosystem Exchange (NEE) or alternatively Net Biosphere Productivity (NBP). This consists of several components. Gross Primary Productivity (GPP) is the uptake of carbon by plants through photosynthesis. Plants also release carbon via respiration, and the difference between GPP and plant respiration is Net Primary Productivity (NPP). Carbon is also released by respiration by microbes in the soil, and by animal life – the difference between NPP and non-plant respiration is Net Ecosystem Productivity (NEP). Carbon is also released through disturbance processes such as fire – the difference between NEP and disturbance emissions is NBP or NEE. NBP / NEE represent the net flux of carbon between the atmosphere and land. The following sections discuss the changes in GPP, NPP and fire emissions in relation to ENSO, and some aspects of regional climate variability that appear to drive these.

3.1.1 Vegetation productivity

NPP is the net carbon uptake by plants including GPP and plant respiration. NPP can be estimated for individual trees by measuring their change in stem diameter, and this can be used to estimate large-scale NPP scaling up large numbers of measurements from individual sites. Using measurements of wood allocation to tree stems (NPP_{stem}) of 8725 tropical trees in 50 sites across 14 regions in the Global Ecosystems Monitoring (GEM) network and a set of site-specific statistical relationships with meteorological variables, Rifai *et al.* (2018) estimated the impacts of climate variability on pan-tropical woody production from 1996 to 2016.

NPP_{stem} shows clear relationships with ENSO in all three major tropical forest areas (Figure 5). With the long-term increasing trend removed for clarity, the 12-month running mean anomaly generally shows declines during periods of warm Niño3.4 SSTs and increases during periods of cool Niño3.4 SSTs. This is evident for periods of small SST anomalies as well as the major anomalies in El Niño and La Niña events. The impacts are generally largest in the Americas and smallest in Africa.

All three major tropical forest areas were impacted to some degree by the major El Niño events in 1997-98 and 2015-16, but the impacts were much larger in the Americas and quite minimal in Africa (Figure 5). NPP_{stem} in the Americas and the Asia-Pacific region were also impacted to some extent by smaller positive Niño3.4 anomalies, particularly 2010-2011. Both of these regions also showed positive NPP_{stem} anomalies in La Niña events, as did Africa in the 2008-09 La Niña.

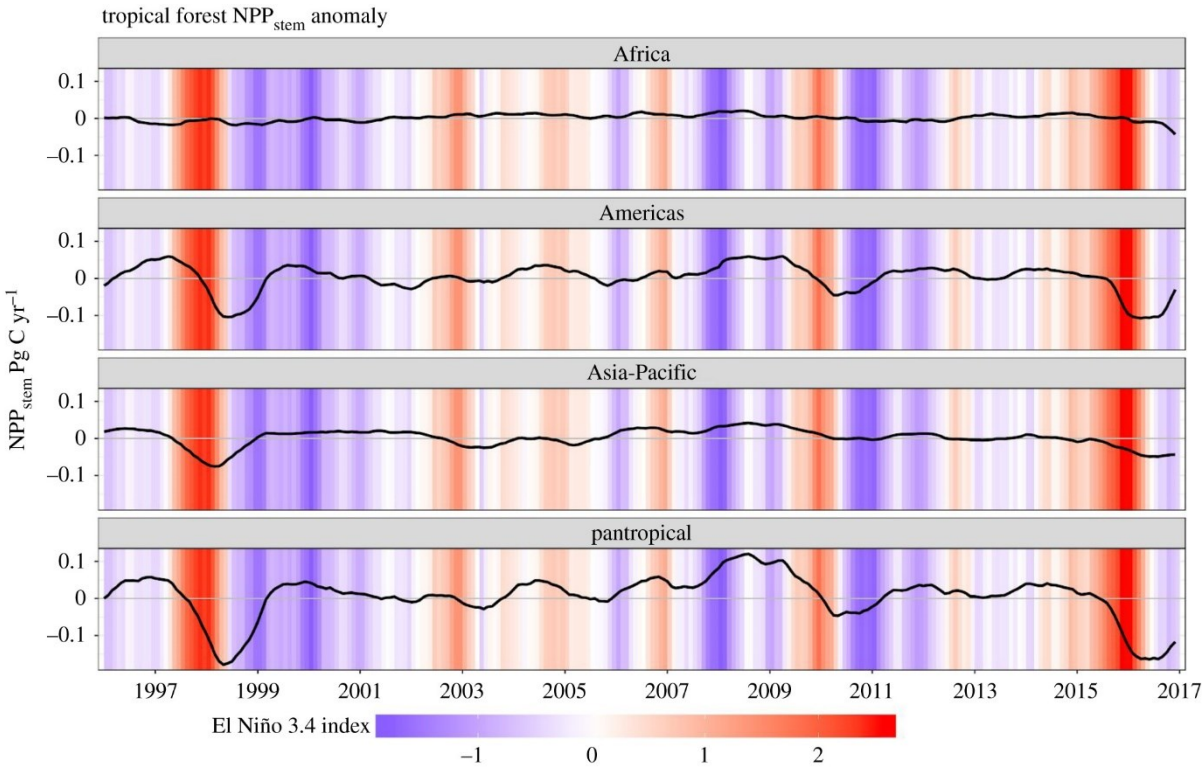

Figure 5. 12-month detrended, running mean anomalies of NPP_{stem} (black) in the three major tropical regions from 1996 to 2017 estimated with a statistical model relating NPP_{stem} to meteorological conditions. Vertical coloured bars show the Niño3.4 index. Reproduced from Rifai *et al.* (2018).

GPP can be estimated with satellite remote sensing with a variety of methods based on the absorption of solar radiation by plants as part of photosynthesis, in combination with other quantities. These often use the fraction of absorbed photosynthetically active radiation, derived from the Normalised Difference Vegetation Index (NDVI) which is a measure of the relative ratios of reflected and incoming radiation in red and near infra-red wavebands. Live vegetation absorbs and reflects red and near infra-red radiation very differently to other surfaces. NDVI is provided by several satellite instruments including the MODerate resolution imaging spectrometer (MODIS) and Advanced Very High Resolution Radiometer (AVHRR).

These data show a general rising trend in GPP from 2000 to 2016 with a reduction in 2015 associated with the El Niño and an increase in 2011 associated with the La Niña (Luo *et al*., 2018) After removing the rising trend in global GPP due to CO_2 fertilization, increased growing season length and other long-terms climate trends, Luo *et el.* (2018) found that global GPP decreased by 0.70 ± 1.20 GtC in 2015, accounting for 60% of the reduction in Net Ecosystem Productivity (NEP). However, in 2016, there was a small increase in GPP of 0.05 ± 0.89 GtC. Since the overall carbon sink still declined in 2016 which cannot be explained by decreased productivity, this implies that the continuation of the weaker net land sink in 2016 was due to increases in carbon release due to respiration or fire.

Variability in large-scale photosynthesis therefore appears to play an important role in the variability of the atmosphere-land CO_2 flux, but is not the only process responsible.

3.1.3 Fire

Global CO_2 emissions from wildfire show a relationship with ENSO, driven predominantly by variability in emissions from tropical regions. Although the details of regional weather in individual events plays an important role, and other factors such as direct human impact via land use, drainage of wetlands and human ignition of fires plays a very large role. The nature of the ecosystems affected by fire is also crucial, with fire in peatlands being particularly important due to very large carbon stocks and hence potential for a high rate of emissions.

Emissions from fire featured prominently in the 1997-98 El Niño event, exceeding 3 GtC yr^{-1}, and since then global fire emissions have fluctuated between approximately 1.8 and 2.3 GtC yr^{-1}, with minima generally in La Niña events and maxima in El Niño (Figure 6a). Generally, global fire emissions are showing a downward trend.

The very large spike in global fire emissions in 1997/98 was almost entirely from Equatorial Asia, more specifically from peatlands in Southeast Asia which were under severe drought and subject to direct human disturbance. Page *et al.* (2002) estimated that between 0.81 and 2.57 GtC were released in 1997, with the upper estimate representing a very large proportion of the global CO_2 flux anomaly estimated from inversion studies (see Figure 8). However, the Global Fire Emissions Database (GFED) gives emissions of 0.53 GtC from Equatorial Asian Peatlands in 1997 (Giglio *et al*., 2013), and this is used in the Global Carbon Budget (eg. Le Quéré *et al*. 2018).

In contrast, in 2015, fires in Indonesia resulted in much lower emissions of 0.35 – 0.60 GtC (Nechita-Banda *et al*, 2018). One reason for the lower emissions compared to 1998-98 is that in 2015 the rains returned in November (GFED). GFED may have overestimated fire in Indonesia in 2015, as the same relationships between burnt area and emissions as used in 1997/98, but now some areas have been repeatedly burnt there is less carbon per unit area to be released (Sue Page – Pers. Commm.) However, ground-based studies in Amazonia suggest GFED underestimates emissions for this region (Withey *et al*., 2018).

Global fire emissions were 2.4 GtC / yr in 2015 and 1.9 GtC / yr in 2016, compared to an average of 2.0 GtC / yr from 2010-2014 (Bastos *et al*., 2018)).

Regional contributions to global fire emissions vary substantially (Figure 6b). Total fire emissions from Africa are consistently high (between 600 and 700 TgC / yr from Northern Hemisphere Africa, and 400 to 600 TgC / yr from Southern Hemisphere Africa), and show relatively little interannual variability. Emissions Southern Hemisphere Africa show a long-term decline. Most other regions have total annual emissions below 200 TgC / yr with relatively small interannual variability. The exceptions are Equatorial Asia and Southern Hemisphere South America, which show large interannual variability with high emissions in El Niño years.

Notably, the Global Carbon Budget dataset of anthropogenic CO_2 emissions shows a clear spike in 1997-98 (Figure 2a), which arises from land use emissions (Figure 3a). This features in the dataset because the peatland fire emissions from Southeast Asia are classed as as anthropogenic (Houghton and Nassikas, 2017) since they were ignited by humans. However the climatic conditions were suitable for fires to run out of control, so the El Niño event played a part too.

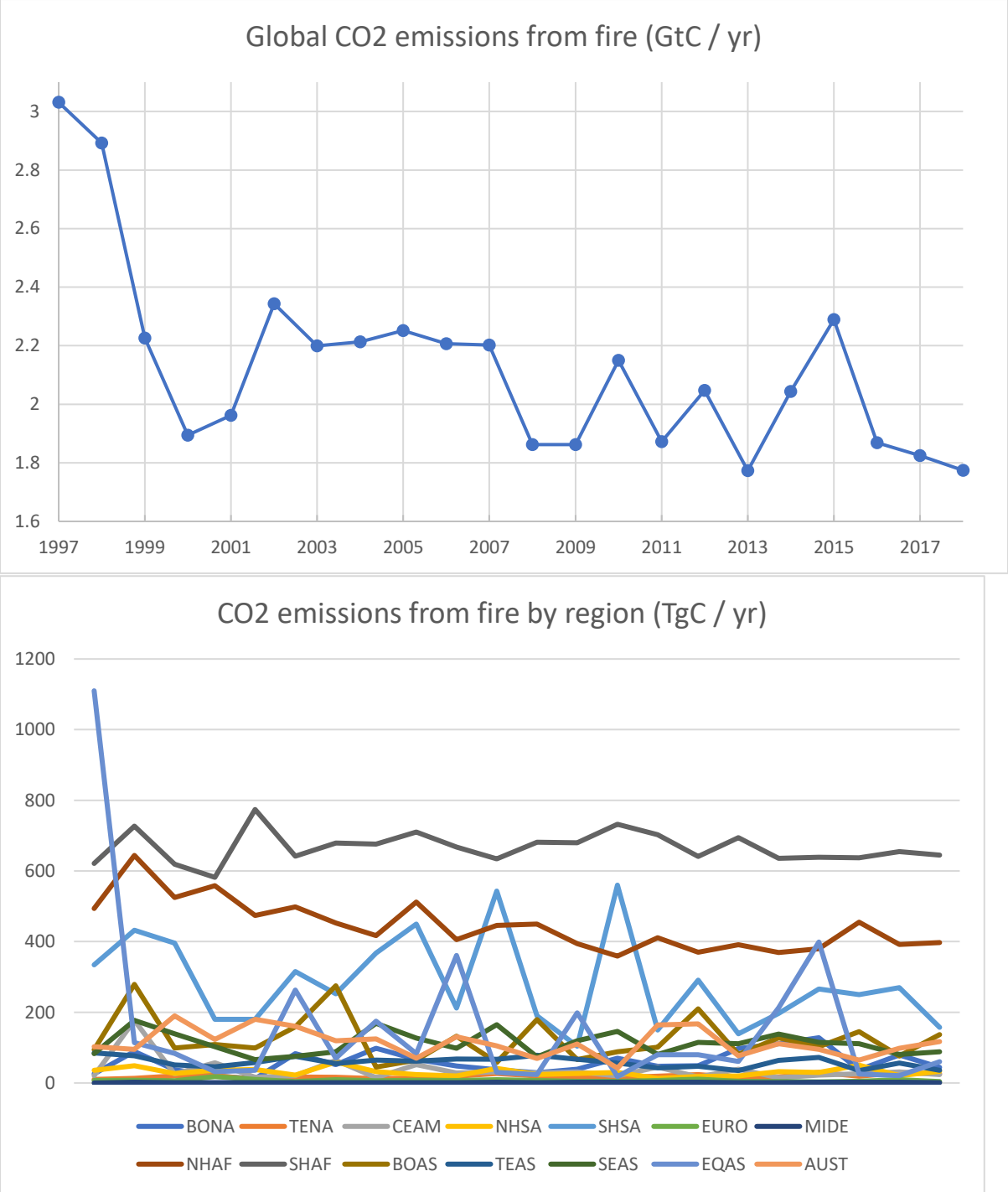

Figure 6 Annual emissions of CO_2 from fire (a) globally and (b) by region. BONA: Boreal North America. TENA: Temperate North America. CEAM: Central America. NHSA: Northern Hemisphere South America. SHSA: Southern Hemisphere South America. EURO: Europe. MIDE: Middle East. NHAF: Northern Hemisphere Africa. SHAF: Southern Hemisphere Africa. BOAS: Boreal Asia. TEAS: Temperate Asia. SEAS: South East Asia. EQAS: equatorial Asia. AUST: Australia and New Zealand. Source: GFED

3.1.4 **Regional climate drivers of land carbon cycle variability**

The global land-atmosphere carbon fluxes are clearly related to ENSO, but what are the climate processes that lead to this connection? Atmospheric CO_2 growth rate is related at the global scale to both land temperature and water availability (Humphrey *et al.*, 2018), with higher growth rates corresponding to warm, dry anomalies (Humphrey *et al.*, 2018). Links to temperature have long been established (Wang *at al.*, 2013). More recently, large-scale estimates of changes in Terrestrial Water Storage (TWS) variability from 2002 to 2017 have become available from satellite remote sensing with GRACE (Gravity Recovery And Climate Experiment) which measured local changes in the Earth's gravity with a pair of satellites. TWS anomalies have also been reconstructed for before the start of the gravimetric measurement period through a modelled relationship with other observed climate variables (Humphrey *et al*., 2017). The resulting TWS timeseries shows a strong inverse correlation with CO_2 growth rate (Figure 7), with generally higher growth rates in years with smaller TWS, which coincide with periods of warm ENSO SST anomalies.

The major exception to this was in 1992/93, when despite a large TWS anomaly showing widespread dry conditions, the CO_2 growth rate was anomalously small. This can be accounted for by the temporary cooling effect of the Mount Pinatubo eruption, which would have been expected to reduce both plant respiration and soil respiration, hence reducing outgassing of CO_2.

Although the TWS-CO_2 relationship is robust, there are some notable differences in the relationship between the two major El Nino events of 1997/98 and 2015/16. In 2015/16 the negative TWS anomaly is the largest on record at over -2 Tt H_2O, and the CO_2 growth rate is the second largest in the record by the measure used in this study. In 1997/98, the global mean TWS anomaly is not substantially larger than many other years, whereas the CO_2 growth rate was the largest in the record by the measure used here. This may suggest that while soil moisture played an important role in 2015/16, other factors were important in the 1997/98 which either amplified the response to soil moisture changes or added to it. For example, the very large store of carbon in Indonesian peatlands meant that the drought-related wildfires released substantial quantities of carbon.

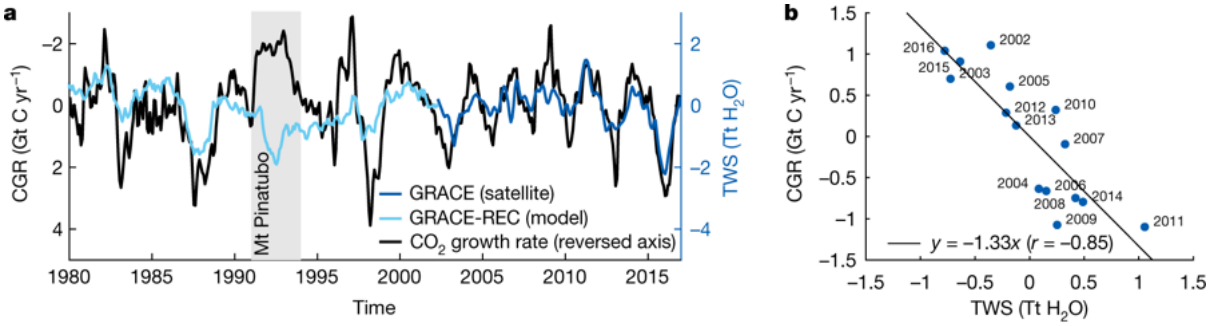

Figure 7 (a) Timeseries of CO_2 growth rate (CGR: black) and terrestrial water storage (TWS) from GRACE satellite measurements (dark blue) and reconstructed from observed climate variables using relationships with GRACE measurements (light blue). (b) Annual CGR versus TWS. Reproduced from Humphrey *et al*. (2018)

In 2015-16, the reductions in GRACE soil moisture were largest in tropical South America, and smaller in southern Africa and South East Asia (Gloor *et al.*, 2018). However, soil moisture may not have been the sole driver of terrestrial carbon cycle changes in 2015/16. Koren *et al.* (2018) suggested that in the Amazon, humidity may have been the strongest driver of GPP impact in 2016, as productivity recovered early in 2016 as atmospheric moisture demand returned to normal levels even though soil moisture drought conditions persisted.

3.2 **Ocean processes**

The interannual variability of the sea-air exchange fluxes in tropical oceans are largely controlled by the variability in partial pressure of CO_2 in the surface waters (pCO_2sw) and the wind forcing influenced by the nature and phasing of the El Niño–Southern Oscillation (ENSO) events, particularly in the tropical Pacific (e.g., Feely *et al*., 1999, 2002, 2006; Ishii *et al*., 2009, 2014; Takahashi *et al*., 2009; Wanninkhof *et al*., 2013; Landschutzer *et al*. 2014, 2016). During non-El Niño and La Niña periods, the central and eastern equatorial Pacific is the major oceanic source of CO_2 to the atmosphere. It is near neutral during strong El Niño periods, and a weak source during weak El Niño periods. The La Niña phase of the ENSO cycle is characterized by strong trade winds, cold tropical SSTs, and enhanced upwelling along the equator. The mean sea-air CO_2 flux based on all observational data is 0.51 ± 0.24 Pg C yr^{-1} for the tropical Pacific, 0.10 Pg C $yr^{-1}$for the tropical Atlantic and 0.1 Pg C yr^{-1} for the tropical Indian Ocean (Takahashi *et al*. 2009; Ishii *et al*., 2014).

The warm El Niño phase of the ENSO cycle is characterized by a large-scale weakening of the trade winds, decrease in upwelling of CO_2 and nutrient-rich subsurface waters and a corresponding warming of SST in the eastern and central equatorial Pacific. The "cold tongue" in the eastern tropics extends to the west during the cold La Niña events and retreats to the east during the warm El Niño events. ENSO drives changes in the distributions of DIC, SST, and salinity in surface water as well as the surface wind field, and causes large perturbations to pCO_2sw and significant temporal variability in the CO_2 outgassing from the tropical Pacific. During the strong eastern Pacific El Niños events of 1982-83, 1997–1998, and 2015-16 the cold waters of the eastern equatorial Pacific disappear and pCO_2 values are close

to equilibrium with the atmosphere. During the weaker central Pacific El Niños of 1991–1994, 2002–2005, and 2006-07 the equatorial cold tongue is present but less pronounced, and pCO_2 values are higher than atmospheric values but lower than corresponding values for non-El Niño periods. These findings are consistent with the westward shift of SST anomalies towards the central Pacific during central Pacific El Niños resulting from weaker upwelling there compared with the stronger SST anomalies in the far eastern Pacific during a strong eastern Pacific El Niño (Landschutzer *et al*., 2016). Figure 8 from Feely *et al*. (2019) presents time-longitude plots of SST and pCO_2 for the region from 5°N to 10°S and 130°E to 95°W, and the Oceanic Niño Index (ONI) for the 36-yr period from 1982 to 2018. The strongest El Niño event of 1997–1998 featured SST anomalies exceeding 4°C and the lowest pCO_2 values throughout most of the equatorial Pacific. In contrast, the 2015-16 El Niño event featured SST anomalies that were similar in magnitude to the 1997-98 event, although the pCO_2 values were significantly higher because the upwelling-favorable winds were stronger in the easternmost and westernmost parts of the region. Recent satellite OCO-2 CO_2 data and mooring-based observations by Chatterjee *et al.* (2017) show that during the early stages of the 2015-2016 ENSO event, atmospheric CO_2 concentrations in the tropical Pacific indicated a flux reduction by 26 to 54% that was due to the decrease in the sea-air CO_2 flux in the tropical Pacific. This was followed by a dramatic increase in atmospheric CO_2 after August 2015 attributed to terrestrial processes as described above..

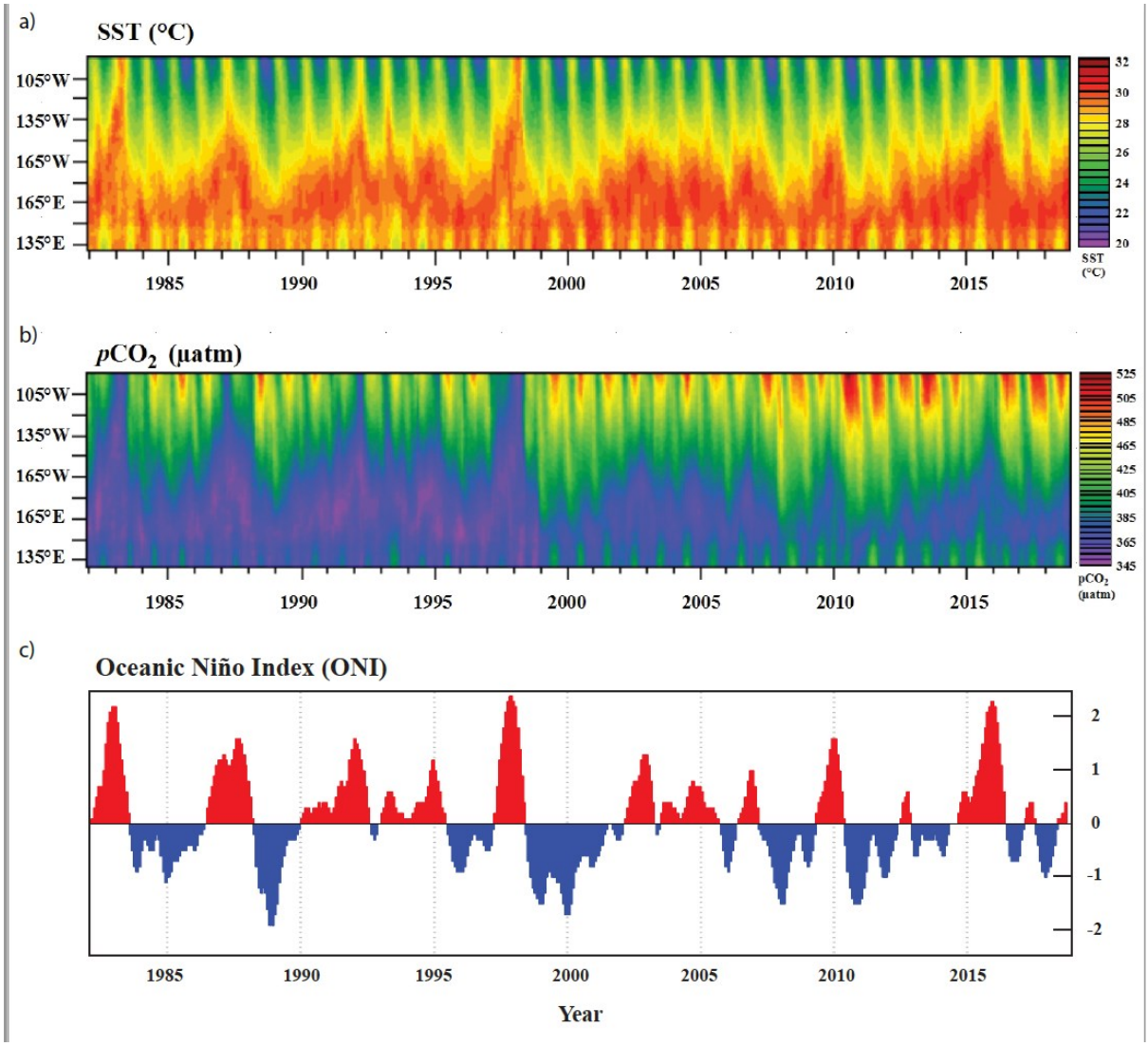

Figure 8. Time-longitude plots of: (a) SST, (b) pCO_2, and the (c) Oceanic Niño Index from 1982 thru 2018 in the equatorial Pacific. Significant reductions in surface water pCO_2 values (low CO_2 outgassing) correspond with the El Niño events of 1982-83, 1986-87,1991-94, 1997-98, 2002-05, 2006-07, 2009-10 and 2015-16. Significant enhancement of the pCO_2 values (high CO_2 outgassing) occurred with the strong La Niña events in 1984-85,1998-99, 1995-96, 1998-2000, 2007-08, and 2011-12. 2018 was a normal non-El Niño year (reproduced from Feely *et al.* 2019).

4 Impacts of major El Niño events on the global carbon cycle

The observed annual CO_2 increment from 2015 to 2016 was 3.39 ppm, the largest in the Maua Loa record. Prior this, the previous largest annual increment was 2.9 ppm between 1997 and 1998. The observed CO_2 annual increment in 2015/16 was therefore substantially larger than that following the previous large El Niño event. How much did each El Niño event contribute to the CO_2 rise, and how much was due to human emissions? Why was the 2015/16 rise larger than 1997/98?

We can make a simple estimate the contribution of specific El Niño events to the annual CO_2 rise by calculating Equation 1 both with the observed SST anomaly for *N* and with no anomaly (ie: *N* = 0) (Betts *et al*., 2018).

Using the observed emissions and SST anomaly, the reconstructed CO_2 increment for 2015/16 is 3.21 ppm (Table 2). In comparison, the observed CO_2 increment was 3.39 ppm. Using a zero SST anomaly, we estimate that the 2016 annual CO_2 increment without El Niño would have been 2.42 ppm, so this method suggests that the El Niño increased the 2016 annual CO_2 increment by 0.79 ppm. We therefore estimate that the El Niño contributed approximately 25% to the record annual CO_2 rise between 2015 and 2016, with the other 75% being due to anthropogenic CO_2 emissions.

For 1997/98 the reconstructed CO_2 increment is 2.59 ppm, and the observed rise was 2.9 ppm. This underestimate might be due the Niño3.4 index being less representative of the magnitude of the 1997/98 El Niño; the Niño3 region might be more representative. The estimated "no El Niño" CO_2 rise is 1.82 ppm, implying an El Niño contribution of 0.77 ppm. This is similar to that for 2015/16 in terms of the absolute contribution, but is a larger proportion (30%) of the overall rise that year.

An important further point for the 1997/98 El Niño is that the anthropogenic emissions itself includes an ENSO-related contribution, as much of the land use emissions were from burning peatlands in South East Asia (Le Quéré *et al*., 2018). Although these were ignited by humans, and hence are counted as anthropogenic in the Global Carbon Budget, the El Niño-related drought provided the conditions for the fires to run out of control and produce very large emissions (Page *et al*., 2002).

The total anthropogenic emissions in 1997 were 8.31 GtC, with 6.53 GtC from fossil fuel combustion and 1.78 GtC from land use change including the Asian peatland fires (Le Quéré *et al*.,2018). By linearly interpolating between the emissions for the previous and following years (1.31 GtC for 1996 and 1.23 GtC for 1998) we estimate that without the El Niño-related peatland fires, global land use emissions in 1997 would have been 1.27 GtC, so total anthropogenic emissions would have been 7.80 GtC. This interpolation implies that the contribution of the Asian peatland fires to anthropogenic land use emissions was 0.51 GtC, close to the total value for Asian peatland fires used in GFED (Giglio *et al*., 2013).

Repeating the estimate of the "no El Niño" CO_2 rise for 1997/98 including this emissions contribution gives a revised figure of 1.71 ppm, so the revised estimate of the El Niño-related contribution to the annual CO_2 increment is 0.88 ppm. This is 34% of the total reconstructed CO_2 rise, so it is estimated that the reduced net carbon sink associated with the 1997/98 El Niño contributed approximately one-third of the CO_2 rise between 1997 and 1998.

Table 2. Estimating the contribution of El Niño to the annual CO_2 increment in 2015/16

	Period	**Observed**	**Calculation with El Niño SSTs**	**Calculation without El Niño SSTs**
N (°C)	April 2015-	1.85 +- 0.19	1.85 ± 0.19	0

	March 2016			
ε (GtC)	January – December 2015	11.1	11.1	11.1
ΔCO_2 (ppm)	2016 – 2015	3.39	3.21	2.42

Table 3. Estimating the contribution of El Niño to the annual CO_2 increment in 1997/98

	Period	**Observed**	**Calculation with El Niño SSTs**	**Calculation without El Niño SSTs**	**Calculation without El Niño SSTs or land use emissions**
N (°C)	April 1997-March 1998	1.81	1.81	0	0
ε (GtC)	January – December 1997	8.3	8.3	8.3	7.8
ΔCO_2 (ppm)	1997 – 1998	2.9	2.59	1.82	1.71

The observed mean CO_2 rise for the decade prior to 2015 was steady at approximately 2.1 ppm/yr, so the rise of 3.39 ppm in one year was a substantial increase. Before 2015, the growth rate did not rise despite an increase in anthropogenic emissions, and this has been attributed increased net uptake of carbon by the terrestrial biosphere due to increased CO_2 fertilization accompanied by a lack of increase in respiration resulting from the temporary slowdown in the rate of global warming [Keenan *et al*., 2106]. We note that our reconstruction of CO_2 increments using equation (1) captures this hiatus in the rate of CO_2 rise between approximately 2003 and 2014 (Figure 18). Since the only climate-related term in equation (1) is the Niño 3.4 SST anomaly, this suggests that the relatively cool conditions in the equatorial Pacific in several of these years may have played a role in the hiatus in the CO_2 rise. La Niña conditions are associated with smaller annual CO_2 rises (Figures 2 and 3), with generally wetter and cooler conditions in many areas. This may be consistent with an emerging understanding of the role of Pacific decadal variability in the global warming hiatus [Meehl *et al*., 2011; Kosaka *et al*., 2013; England *et al*., 2014].

Therefore, although the large increase in CO_2 rise in 2015/16 was largely associated with the El Niño, there was also probably a contribution from the cessation of the anomalously slow rate of rise associated with cooler conditions in the tropical Pacific.

It therefore appears that the main reason why the CO_2 annual increment in 2015-16 was larger than 1997-98 is that anthropogenic emissions from fossil fuel burning increased substantially in that period. Although land use emissions including fire made a smaller contributed to the CO_2 rise in 2015/16 compared to 1997/98, total anthropogenic emissions including fossil fuel burning had risen by 2.7 GtC between 1997 and 2015 (an increase of over 30%).

5 Role of ENSO in predicting the future behaviour of the Earth System

5.1 Forecasting the CO_2 rise on annual timescales

Since the annual CO_2 growth rate is closely linked to ENSO, and ENSO has some predictability (see Chapter 10), this means that it is possible to make successful forecasts of the annual CO_2 rise ahead of time (Betts *et al*., 2016; Betts *et al.*, 2018). Such forecasts are now a routine product from the Met Office [https://www.metoffice.gov.uk/news/releases/2019/2019-carbondioxide-forecast]. These provide a useful learning experience for testing understanding of climate-carbon cycle links – making a specific prediction and then looking closely at the reasons for success or failure can be instructive. Also, the ongoing rise in CO_2 is of interest to those members of the public, media and policy world who are concerned with anthropogenic climate change, so making and testing predictions of the CO_2 concentration can provide a tool for raising awareness.

The Met Office forecast method uses the statistical relationship between the annual CO_2 increment, emissions and equatorial Pacific SSTs in Equation (1). The forecast is calculated in November using annual emissions from the Global Carbon Project for the current calendar year (which includes a projection for the end of the year), and Niño3.4 SSTs from HadISST observations [Kennedy *et al*., 2011a, 2011b] from the preceeding April to October combined with a forecast of SSTs from the GloSea climate model (MacLachlan *et al*., 2015) for the coming November to March. These are used to calculate the predicted increment in annual mean atmospheric CO_2 concentration at Mauna Loa from the current year to the following year. This is then used to forecast the annual mean CO_2 concentration across the following year. Using an assumption of a uniform seasonal cycle, the monthly mean CO_2 concentrations are also predicted, with a particular focus on the annual maximum monthly concentration in May and the annual minimum monthly concentration in September (Betts *et al*., 2018).

The Mauna Loa measurements are chosen as the focus of the Met Office CO_2 forecast as they provide a very specific, precisely-measured quantity – in contrast, the global mean CO_2 concentration relies on estimates and assumptions, which introduce additional uncertainties. Although CO_2 is measured at other sites, Mauna Loa is the original measurement site and provides the longest record as well as being of historic interest.

The Met Office CO_2 forecast was first produced in 2015, predicting the annual increment between that year and 2016 (Betts *et al*., 2016). This was of particular interest for two reasons: (i) the large El Niño emerging in late 2015, and (ii) atmospheric CO_2 concentrations being around 400ppm – not a threshold of physical significance, but nevertheless a symbolic threshold as rising concentrations passed from the 300s to the 400s. Since then, the CO_2 forecast has been issued on an annual basis.

The CO_2 rise in 2016 was successfully forecast to be the largest on record (Table 4), due to the amplifying effects of the 2015/2016 El Niño event (Betts *et al*., 2018). The rises in 2017 and 2018 were successfully forecast to be more moderate, due to neutral Niño3.4 SSTs in 2016-17 and La Niña conditions in 2017-18. The forecast for 2019, issued in January 2019 during

the preparation of this chapter, was for a return to a larger annual increment (but not as large as 2015-16) due to the predicted moderate El Niño. At the time of going to press, the concentrations forecast for the first months of 2019 were accurate.

Table 4. Summary of forecast and observed CO_2 concentrations and rises for 2016, 2017 and 2018, and the forecast for 2019.

	Annual mean CO_2 concentration (ppm)		**Increase from previous year (ppm)**		**May maximum (ppm)**		**September minimum (ppm)**	
Year	**Forecast**	**Observed**	**Forecast**	**Observed**	**Forecast**	**Observed**	**Forecast**	**Observed**
2019	411.3±0.58		2.74±0.58		414.7±0.58		408.1±0.58	
2018	408.94±0.59	408.59	2.29±0.59	2.00	412.20±0.59	411.31	405.79±0.59	405.59
2017	406.75±0.61	406.59	2.46±0.61	2.31	409.86±0.61	409.91	403.72±0.61	403.27
2016	404.45±0.53	404.28	3.15±0.53	3.39	407.57±0.53	407.65	401.48±0.53	401.01

An area for possible methodological improvement of the CO_2 forecast concerns the assumption of a stationary seasonal cycle. Since the shape of seasonal CO_2 cycle varies, this is a potential shortcoming with the monthly forecasts. However, the amplitude of the seasonal cycle shows less variation, so the prediction of annual maxima and minima appears to be robust.

5.2 Carbon cycle – ENSO relationships in Earth System Models

Since coupled ocean-atmosphere general circulation models (GCMs) project ENSO events to become more frequent and intense (Cai *et al*., 2015; see Chapter 13), it is important to understand the potential implications of this for the carbon cycle and hence as a feedback process on anthropogenic climate change. Now that the carbon cycle is now routinely included in GCMs as part of their evolution into Earth System Models (ESMs), this provides an opportunity to examine the role of ENSO-carbon cycle interactions in long-term climate change.

The relationship between ENSO and interannual variability in the carbon cycle emerges in ESMs (Jones *et al.*, 2001; Kim *et al*., 2016), and hence is evidence of realistic behaviour of such models on these timescales. The CMIP5 generation of ESMs simulate the observed ENSO-carbon cycle relationship reasonably well in terms of magnitude, timing and the processes involved. Considering the onset and decline of the atmospheric CO_2 growth rate anomaly within an El Niño event, the multi-model mean overestimates the maximum growth rate by approximately 20%, and the peak growth rate is correctly simulated to occur in the boreal spring but at around April rather than January as observed (Kim *et al*., 2016). The growth rate

anomalies are caused mainly by variability in NPP, in agreement with the indications from observationally-based studies as described earlier in this chapter.

In the CMIP5 ESMs, the sensitivity of the terrestrial carbon flux to ENSO is projected to increase by 44% (± 15%) in a scenario of CO_2 concentrations stabilised at around 540 ppm, ie: nearly double the pre-industrial concentration (Kim *et al.*, 2017). The response of land temperature to ENSO and the response of GPP to land temperature are both projected to increase under the warmer climate, with the depletion of soil moisture increasing the temperature response to ENSO events.

Cox *et al.* (2013) and Wenzel *et al*. (2014) suggested that the relationship between interannual variability in CO_2 growth rate and tropical temperature could provide a constraint on a key component of carbon cycle feedbacks on climate change (Figure 9), although clearly this depends on whether similar processes are involved on interannual and longer-term timescales. In two generations of Earth System Models (C^4MIP and CMIP5), the sensitivity of annual growth rate to temperature on annual timescales correlates strongly with the response of tropical land carbon storage to climate change (Figure 9a). Comparison with the observed CO_2-temperature relationship on annual timescales can therefore be used to estimate the probability distribution of tropical land carbon responses to climate change (Figure 9b).

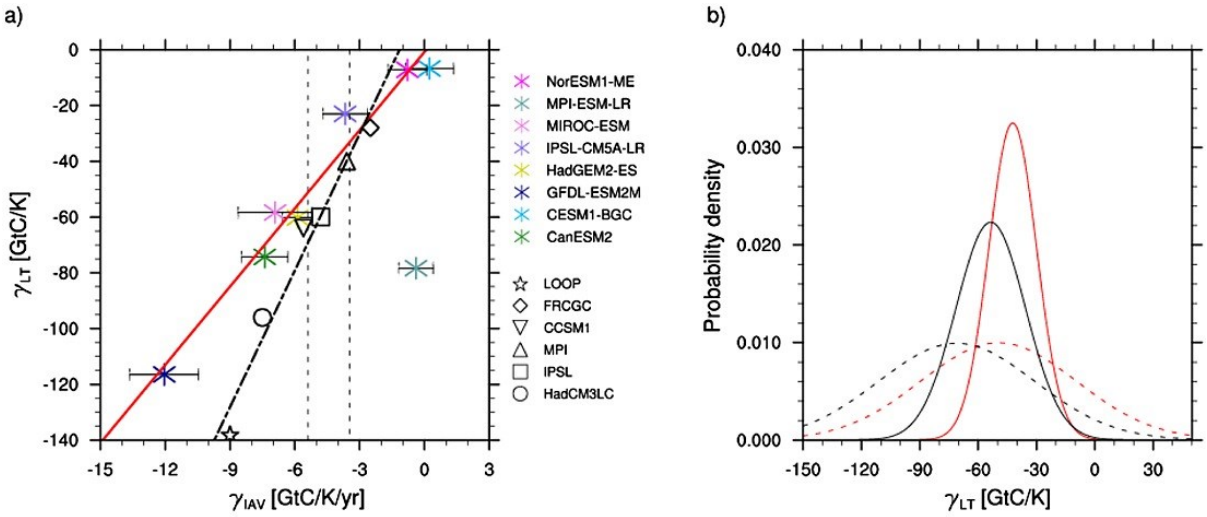

Figure 9. Use of interannual variability in CO_2 growth rate and tropical temperature as a constraint on carbon cycle feedbacks on climate change. (a) strength of feedback on climate change vs. sensitivity of annual growth rate to temperature on annual timescales in Earth System Models from C_4MIP (black symbols, best fit shown with dot-dashed black line) and CMIP5 (coloured stars, best fit shown with solid red line), with observational constraint on the interannual growth rate (vertical black dashed lines). (b) probability distribution of feedback strengths from unconstrained ESMs (dashed curves) and after constraint by comparison with observed interannual variability (solid curves), for C^4MIP (red) and CMIP5 (black) ESMs. Reproduced from Wenzel *et al*., (2014)

Without the ENSO constraint, there is a large spread in the projected loss of tropical land carbon (-49 ± 40 GtC per °C of tropical land warming) (Figure 8b). The ENSO constraints narrows this to -44 ± 14 GtC/°C.

6 **Summary and conclusions**

A wealth of observational studies of atmospheric CO_2, land ecosystem and ocean processes show that variability in the carbon cycle is closely related with ENSO. Years with a warm anomaly in the tropical Pacific show a faster CO_2 rise due to weaker land carbon sinks, with a partial offset by stronger net uptake by oceans. The opposite happens in years with cool Pacific SST anomalies. This relationship holds for small ENSO SST anomalies as well as large ones, and is robust enough for the annual CO_2 growth rate anomaly to be highly predictable on the basis of SST observations and forecasts.

Generally, variability in the land-atmosphere carbon flux is mainly driven by physiological processes – photosynthesis and/or respiration responses to temperature and precipitation – with a smaller contribution from fire. Fire was important in the 1997-98 El Niño, with Equatorial Asian peatland fires making a major contribution to the CO_2 rise which can be viewed as anthropogenic in nature since the ignition was caused by humans. However, in the 2015-16 El Niño event, the change in land carbon flux was mainly due to physiological processes, particularly reduced productivity, although this does not provide a complete explanation so increased respiration may also have played a role. In El Niño years, net CO_2 release from tropical land is the most immediate impact, followed by release from northern ecosystems a few months later. The lag between peak SST anomaly and peak CO_2 growth rate anomaly varies according to whether the SST anomaly is in the Central or Eastern Pacific.

In the oceans, El Niño conditions involve decreased upwelling of carbon in the equatorial Pacific due to a weakening of the trade winds, causing this region to become a weaker sink of CO_2 or near-neutral if the El Niño event is strong.

ENSO-carbon cycle relationships beyond individual years are also seen. In the late 2000s to early 2010, the annual increase in CO_2 concentration remained approximately steady rather than generally rising as it had done before and has done since. A statistical relationship with tropical Pacific SSTs reproduces this, with a dominance of La Niña conditions in the late 2000s-early 2010s, and global land carbon uptake anomalously high in that period, suggesting the relationship with ENSO acting via land ecosystem carbon sinks was responsible for this hiatus in the rise of the global CO_2 growth rate.

Earth System Models also reproduce the ENSO - carbon cycle relationship well, and this has been proposed as a useful constraint on carbon cycle feedbacks in future climate change projections. Earth System Models project the carbon cycle to become more responsive to ENSO under future climate change, and with ENSO events projected to become more frequent and intense, this may lead to carbon cycle feedbacks accelerating anthropogenic climate change.

References

Bacastow, R.B. (1976) Modulation of atmospheric carbon dioxide by the Southern Oscillation. *Nature*, 261, 116–118

Bacastow, R.,B., Adams, J.A., Keeling, C.D., Moss, D.J., Whorf, T.P. & Wong, C.S. (1980) Atmospheric carbon dioxide, the southern oscillation, and the weak 1975 El Nino. *Science*, 210, 66–68

Bakker, D.C.E. (2016) A multi-decade record of high-quality fCO_2 data in version 3 of the Surface Ocean CO_2 Atlas (SOCAT), Earth Syst. Sci. Data, 8, 383–413, https://doi.org/10.5194/essd-8-383-2016

Bastos, A., Friedlingstein, P., Sitch, S., Chen, C., Mialon, A., Wigneron, J-P., *et al.* (2018) Impact of the 2015/2016 El Niño on the terrestrial carbon cycle constrained by bottom-up and top-down approaches. *Phil. Trans. R. Soc. B* **373**, 20170304.

Battle, M., Fletcher, S.E.M., Bender, M.L., Keeling, R.F., Manning, A.C., Gruber, N., et al. (2006) Atmospheric potential oxygen: New observations and their implications for some atmospheric and oceanic models. Global Biogeochemical Cycles. 20

Betts, R.A., Jones, C.D., Knight, J.R., Keeling, R.F., Kennedy, J.J. (2016) El Niño and a record CO_2 rise. *Nature Climate Change* **6**, 806–810, doi:10.1038/nclimate3063

Betts, R.A, Jones, C.D., Knight, J.R., Keeling, R.F., Kennedy, J.J., Wiltshire, A.J., Andrew, R.M., Aragao LEOC. (2018) A successful prediction of the record CO_2 rise associated with the 2015/2016 El Niño. *Phil. Trans. R. Soc. B* **373**, 20170301.

Burton, C. (2019) Impacts of fire, climate and land-use change on terrestrial ecosystems. PhD thesis, University of Exeter.

Burton C., Betts, R.A., Cardoso, M., Feldpausch, T. R., Harper, A., Jones, C., Kelly, D.I., Robertson, E., Wiltshire, A. (2018). Representation of disturbance in the Joint UK Land Environment Simulator Vn4.8 (JULES). Geosci. Model Dev. Discuss., http://doi.org/10.5194/gmd-2018-149

Cai, W., Santoso, A., Wang, G., Yeh, S-W., An, S-I., Cobb, K.M., *et al.* (2015) ENSO and greenhouse warming. *Nature Climate Change*, 5, 849–859

Chatterjee, A., Gierach, M.M., Sutton, A.J., Feely, R.A., Crisp, D., Eldering, A. et al, (2017): Influence of El Niño on atmospheric CO_2 over the tropical Pacific Ocean: Findings from NASA's OCO-2 mission. *Science*, *358*(6360), eaam5776, doi: 10.1126/science.aam5776.

Chylek, P., Tans, P., Christy, J. and Dubey, M. K. (2018) The carbon cycle response to two El Nino types: an observational study. *Environ. Res. Lett.* **13** 024001

Cox P.M., Betts R.A., Jones C.D., Spall S.A., Totterdell I.J. (2000) Acceleration of global warming due to carbon-cycle feedbacks in a coupled climate model. *Nature* **408**, 184–187.

Cox, P.M., Pearson, D., Booth, B.B., Friedlingstein, P., Huntingford, C., Jones, C.D., Luke, C.M. (2013) Sensitivity of tropical carbon to climate change constrained by carbon dioxide variability. Nature 494, 341–344 (2013).

England, M. H., McGregor, S., Spence, P., Meehl, G.A., Timmermann, A., Cai, W. et al. (2014) Recent intensification of wind-driven circulation in the Pacific and the ongoing warming hiatus, Nature Climate Change, 4, 222-227, doi: 10.1038/nclimate2106

Feely, R.A., R. Wanninkhof, T. Takahashi, and P. Tans (1999): Influence of El Niño on the equatorial Pacific contribution of atmospheric CO_2 accumulation. Nature, 398, 597–601, doi: 10.1038/19273.

Feely, R.A., J. Boutin, C.E. Cosca, Y. Dandonneau, J. Etcheto, H.Y. Inoue, et al. (2002) Seasonal and interannual variability of CO_2 in the equatorial Pacific. Deep-Sea Res. Pt. II, 49(13–14), 2443–2469, doi: 10.1016/S0967-0645(02)00044-9.

Feely, R.A., T. Takahashi, R. Wanninkhof, M.J. McPhaden, C.E. Cosca, S.C. Sutherland, and M.-E. Carr (2006): Decadal variability of the air-sea CO_2 fluxes in the equatorial Pacific Ocean. J. Geophys. Res., 111(C08), C08S90, doi: 10.1029/2005JC003129.

Feely, R.A., Wanninkhof, R., Carter, B.R., Landschützer, P., Sutton, A.J., Cosca, C. and Triñanes, J.A. (2019) Global ocean carbon cycle. In *State of the Climate in 2018*, Global Oceans. *Bull. Am. Meteorol. Soc.*, *100*(9), S94–S99, doi: 10.1175/2019BAMSStateoftheClimate.1.

Giglio, L., Randerson, J.T., and van der Werf, G. R. (2013) Analysis of daily, monthly, and annual burned area using the fourth-generation global fire emissions database (GFED4). Journal of Geophysical Research: Biogeosciences, 118, 317–328, doi:10.1002/jgrg.20042, 2013

Gloor E., Chris Wilson, Chipperfield, M.P., Chevallier, F., Buermann, W., Boesch, H.,*et al*., 2018 Tropical land carbon cycle responses to 2015/16 El Niño as recorded by atmospheric greenhouse gas and remote sensing data. Phil. Trans. R. Soc. B 373: 20170302.

Houghton, R. A., and Nassikas, A.A. (2017), Global and regional fluxes of carbon from land use and land cover change 1850–2015, Global Biogeochem. Cycles, 31, 456–472, doi:10.1002/ 2016GB005546.

Humphrey, V., Zscheischler, J., Ciais, P., Gudmundsson, L., Sitch, S. and Seneviratne, S.I. (2018) Sensitivity of atmospheric CO_2 growth rate to observed changes in terrestrial water storage. Nature, 560(7720): 628-631.

Ishii, M., Inoue, H.Y., Midorikawa, T., Saito, S., Tokieda T., Sasano, D., et al. (2009) Spatial variability and decadal trend of the oceanic CO_2 in the western equatorial Pacific warm/fresh water. Deep-Sea Res. II, 56(8–10), 591–606, doi: 10.1016/j.dsr2.2009.01.002.

Ishii, M., Feely, R.A., Rodgers, K.B., Park, G.-H, Wanninkhof, R., Sasano, D. *et al.* (2014): Air-sea CO_2 flux in the Pacific Ocean for the period 1990-2009. Biogeosciences, 11, 709–734, doi: 10.5194/bg-11-709-2014.

Jones, C. D., Collins, M., Cox, P.M. & Spall, S.A. (2001) The carbon cycle response to ENSO: A coupled climate-carbon cycle model study, *J. Clim.*, 14, 4113 – 4129

Jones, C.D., and Cox, P.M. (2001) Modeling the volcanic signal in the atmospheric CO_2 record. Global Biogeochemical Cycles 15, 453-465

Jones, C.D. and Cox, P.M. (2005) On the significance of atmospheric CO_2 growth rate anomalies in 2002–2003, *Geophys. Res. Lett.*, 32, L14816, doi:10.1029/2005GL023027

Jung M., Reichstein M., Schwalm C.R., Huntingford C., and Sitch S. (2017) Compensatory water effects link yearly global land CO_2 sink changes to temperature. *Nature* **541**, 516.

Keeling, R.F. and Manning, A.C. (2014) *Studies of recent changes in atmospheric O2 content.* In: Treatise on Geochemistry. . Reference Module in Earth Systems and Environmental Sciences, 5 . Elsevier, Amsterdam, pp. 385-404.

Keeling C.D. and Revelle R. (1985) Effects of El-Niño southern oscillation on the atmospheric content of carbon-dioxide. *Meteoritics* **20**, 437–450.

Keeling, C.D., Piper, S.C., Bacastow, R.B., Wahlen, M., Whorf, T.P., Heimann, M. and Meijer, H.A. (2001) Exchanges of atmospheric CO_2 and $13CO_2$ with the terrestrial biosphere and oceans from 1978 to 2000. I. Global aspects, SIO Reference Series, No. 01-06, Scripps Institution of Oceanography, San Diego, 88 pages.

Keenan, T.F., Prentice, I.C., Canadell, J.G., Williams, C.A., Wang, H., Raupach, M., Collatz, G.J. (2016) Recent pause in the growth rate of atmospheric CO_2 due to enhanced terrestrial carbon uptake. *Nature Communications* **7**, 13428. doi:10.1038/ncomms13428

Kennedy J.J., Rayner, N.A., Smith, R.O., Saunby, M. and Parker, D.E. (2011a). Reassessing biases and other uncertainties in sea-surface temperature observations since 1850 part 1: measurement and sampling errors. J. Geophys. Res., 116, D14103, doi:10.1029/2010JD015218

Kennedy J.J., Rayner, N.A., Smith, R.O., Saunby, M. and Parker, D.E. (2011b). Reassessing biases and other uncertainties in sea-surface temperature observations since 1850 part 2: biases and homogenisation. J. Geophys. Res., 116, D14104, doi:10.1029/2010JD015220

Kim, J.S. and Kug, J.S. (2016) Increased Atmospheric CO_2 Growth Rate during El Niño Driven by Reduced Terrestrial Productivity in the CMIP5 ESMs. Journal of Climate, 29, 8783-8805

Kim, J-S., Kug, J-S., and Jeong, S-J. (2017) Intensification of terrestrial carbon cycle related to El Niño–Southern Oscillation under greenhouse warming. *Nature Communications*, 8, Article number: 1674

Khatiwala, S., Tanhua, T., Mikaloff Fletcher, S., Gerber, M., Doney, S. C., Graven, H. D. (2013) Global ocean storage of anthropogenic carbon, Biogeosciences, 10, 2169–2191, https://doi.org/10.5194/bg-10-2169-2013

Kosaka Y, Xie S-P. (2013) Recent global-warming hiatus tied to equatorial Pacific surface cooling. Nature.501:403–7.

Kriegler, E., Hall, J. W., Held, H., Dawson, R. and Schellnhuber, H.-J. (2009) Imprecise probability assessment of tipping points in the climate system. *PNAS* 106 (13) 5041-5046; https://doi.org/10.1073/pnas.0809117106

Landschützer, P., Landschützer, P., Gruber, N., Bakker, D. C. E., Schuster, U., Nakaoka, S., Payne, M. R. (2013) A neural network-based estimate of the seasonal to inter-annual variability of the Atlantic Ocean carbon sink. Biogeosciences, 10, 7793-7815, doi:10.5194/bg-10-7793-2013.

Landschützer, P., Gruber, N., Bakker, D.C.E., and Schuster, U. (2014) Recent variability of the global ocean carbon sink. Global Biogeochemical Cycles, 28, 927-949, doi: 10.1002/2014gb004853.

Landschützer, P., Gruber, N., and Bakker, D.C.E. (2016) Decadal variations and trends of the global ocean carbon sink, Global Biogeochem. Cycles, 30, 1396–1417, doi:10.1002/2015GB005359.

Le Quéré, C., Andrew, R.M., Friedlingstein, P., Sitch, S., Hauck, J., Pongratz, J., et al (2018), Global Carbon Budget 2018. Earth System Science Data, 10, 1-54, 2018, DOI: 10.5194/essd-10-2141-2018.

MacLachlan, C., Arribas, A., Peterson, K.A., Maidens, A., Fereday, D., Scaife, A.A., *et al.* (2015) Description of GloSea5: the Met Office high resolution seasonal forecast system. Q. J. R. Met. Soc., DOI: 10.1002/qj.2396.

Malhi, Y., Rowland, L., Aragão, L.E.O.C, and Fisher R.A. (2018) New insights into the variability of the tropical land carbon cycle from the El Niño of 2015/2016. Phil. Trans. R. Soc. B 373: 20170298. http://dx.doi.org/10.1098/rstb.2017.0298

McNeil, B. I., Matear, R. J., Key, R. M., Bullister, J. L., and Sarmiento, J. L. (2003) Anthropogenic CO_2 uptake by the ocean based on the global chlorofluorocarbon data set, Science, 299, 235–239, https://doi.org/10.1126/science.1077429

Meehl G.A., Washington W.M. (1996) El Niño-like climate change in a model with increased atmospheric CO_2 concentrations. *Nature* 382: 56–60

Meehl, G.A., Arblaster, J.M., Fasullo, J.M., Hu, A. and Trenberth, K.E. (2011) Model-based evidence of deep-ocean heat uptake during surface-temperature hiatus periods. *Nature Climate Change*, doi:10.1038/nclimate1229

Mikaloff Fletcher, S. E., Gruber, N., Jacobson, A. R., Doney, S. C., Dutkiewicz, S., Gerber, M. (2006) Inverse estimates of anthropogenic CO_2 uptake, transport, and storage by the oceans, Global Biogeochem. Cy., 20, GB2002, https://doi.org/10.1029/2005GB002530

Page, S.E. Siegert, F., Rieley, J.O., Boehm, H-D.V., Jayak, A. and Limink, S. (2002) The amount of carbon released from peat and forest fires in Indonesia during 1997. *Nature* 420, 61-65

Palmer P.I. (2018) The role of satellite observations in understanding the impact of El Niño on the carbon cycle: current capabilities and future opportunities. *Phil. Trans. R. Soc. B* **373**, 20170407.

Rayner, P. J., and Law, R.M. (1999) The interannual variability of the global carbon cycle. *Tellus*, **51B**, 210–212, doi:https://doi.org/10.1034/j.1600-0889.1999.t01-1-00007.x

Rayner, P. J., Law, R.M. and Dargaville, R. (1999) The relationship between tropical CO_2 fluxes and the El Niño–Southern Oscillation. *Geophys. Res. Lett.*, **26**, 493–496, doi:https://doi.org/10.1029/1999GL900008.

Rifai, S.W., Girardin, C.A.J., Berenguer, E., del Aguila-Pasquel, J., Dahlsjö, C.A.L., Doughty, C.E. *et al.* (2018) ENSO Drives interannual variation of forest woody growth across the tropics. Phil. Trans. R. Soc. B 373: 20170410.

Rödenbeck, C., Zaehle, S., Keeling, R., Heimann, M. (2018) History of El Niño impacts on the global carbon cycle 1957–2017: a quantification from atmospheric CO2 data. *Phil. Trans. R. Soc. B* **373**, 20170303.

Santoso, A., Mcphaden, M. J., and Cai, W. (2017). The defining characteristics of ENSO extremes and the strong 2015/2016 El Niño. Reviews of Geophysics, 55, 1079–1129. https://doi.org/10.1002/2017RG000560

Takahashi, T., Sutherland, S.C., Wanninkhof, R., Sweeney, C., Feely, R.A., Chipman, D.W. *et al.* (2009) Climatological mean and decadal change in surface ocean pCO_2, and net sea-air CO_2 flux over the global oceans. Deep-Sea Res. II, 56(8–10), 554–577, doi: 10.1016/j.dsr2.2008.12.009.

van der Werf, G. R., Randerson, J. T., Giglio, L., van Leeuwen, T. T., Chen, Y., Rogers, B. M., (2017) Global fire emissions estimates during 1997–2016, Earth Syst. Sci. Data, 9, 697-720, https://doi.org/10.5194/essd-9-697-2017.

Wang, J., Zeng, N., Wang, M., Jiang, F., Wang, H., and Jiang, Z. (2018) Contrasting terrestrial carbon cycle responses to the 1997/98 and 2015/16 extreme El Niño events. Earth System Dynamics, 9(1), 1-14. https://doi.org/10.5194/esd-9-1-2018.

Wang, W., Ciais, P., Nemani, R.R., Canadell, J.P., Piao, S., Sitch, S. *et al.* (2013) Variations in atmospheric CO_2 growth rates coupled with tropical temperature. *Proc. Natl Acad. Sci. USA* **110**, 13 061–13 066.

Wanninkhof, R., G.-H. Park, T. Takahashi, C. Sweeney, R. Feely, Y. Nojiri, *et al.* (2013) Global ocean carbon uptake: Magnitude, variability, and trends. Biogeosciences, 10, 1983–2000, doi: 10.5194/bg-10-1983-2013.

Wenzel, S., Cox, P.M., Eyring, V., and Friedlingstein, P. (2014), Emergent constraints on climate-carbon cycle feedbacks in the CMIP5 Earth system models, J. Geophys. Res. Biogeosci., 119, 794–807, doi:10.1002/2013JG002591

Withey, K., Berenguer, E., Palmeira A.F., Espírito-Santo, F.D. B., Lennox, G.D., Silva, C.V. J., *et al.* (2018) Quantifying immediate carbon emissions from El Niño-mediated wildfires in humid tropical forests *Philosophical Transactions of the Royal Society B: Biological Sciences, 373,* http://doi.org/10.1098/rstb.2017.0312